Published by :
http://www.ijert.org

International Journal of Engineering Research & Technology (IJERT)
ISSN: 2278-0181
Vol. 5 Issue 01, January-2016

Effects of a Coarse Grain Matrix Phase in AA 6061-Tic Nanocomposites on Microstructure, Cold Workability and Strain Hardening Behaviour

D. Jeyasimman
Department of Mechanical Engineering,
Periyar Maniammai University,
Thanjavur - 613403,
Tamil Nadu, India.

Ujendra Kumar Komal
Department of Mechanical & Industrial Engineering,
Indian Institute of Technology
Roorkee, 247667, Uttarkhand, India.

R. Narayanasamy
Department of Production Engineering,
National Institute of Technology,
Tiruchirappalli-620015, Tamil Nadu, India.

Abstract **- Nanocrystalline AA 6061 alloy powders reinforced with 2 weight percentage (wt.%) TiC nanoparticles were blended with 0, 5, 10, 15, 20 and 25 wt.% coarse grain elemental powders related to AA 6061 alloy composition to produce a trimodal microstructure via mechanical alloying. The trimodal composite powders were consolidated at 500 MPa and sintered at 798 K for 6 h under a N_2 atmosphere. The sintered composite preforms were characterised by optical microscopy. The room temperature compressive deformation behaviour was evaluated under a triaxial stress state condition. It was found that there was a gradual improvement in the compressive ductility as the percentage of the coarse grain phase increased in the nanocomposites. It was also found that the cold workability percentage of the 25 wt.% coarse grain trimodal composite was approximately five times higher than that of the 0 wt.% coarse grain composite.**

Key words; Nanocomposite; Trimodal; Cold workability; Strain hardening behaviour

I. INTRODUCTION

Aluminium-based metal matrix composites (MMCs) reinforced with ceramic particles are of great interest because of the combined effects of metallic and ceramic materials relative to the corresponding monolithic alloys [1]. The resulting materials have a wide variety of applications, including aerospace, automotive, defence and structural applications, because of their higher elastic modulus, tensile strength, fatigue and wear resistance in comparison with unreinforced alloys [2]. However, reinforcement using ceramic particles such as Al_2O_3 and TiO_2 further reduces the material ductility. To improve the ductility while maintaining considerable strength and toughness of nanocrystalline/nanocomposite materials at room temperature regime, the concept of trimodaled composite has been developed. Trimodal Al-based composites consisting of a nanocrystalline (NC) Al 6061 phase reinforced with TiO_2 and B_4C along with a coarse grain (CG) Al phase have been investigated by various authors [3-6].As an effective approach towards obtain in high strength and good ductility, bimodal/trimodal grain size distributions in nanostructured alloys have become attractive in the last decade [7]. In trimodal Al MMCs, the reinforcement and the NC phase provide the high strength characteristics of composites, and the CG Al phase is introduced to improve the ductility [8-9].The schematic diagram of incorporating CG into nanostructured materials before and after cold upsetting (Trimodalled microstructure) is shown in Fig. 1.

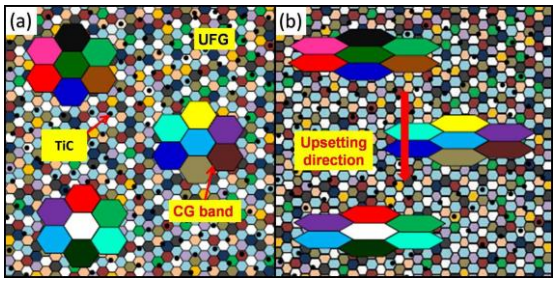

Fig.1. Incorporating coarse-grains to improve the ductility of nanocrystalline materials by consolidation of blended coarse grains powders: (a) before upsetting and (b) after upsetting

Of all of the aluminium alloys, AA 6061 is a popular choice as a matrix material for the preparation of MMCs. These materials have good formability and heat treatability properties. In the present work, TiC nanoparticles were used as reinforcements because of their high melting temperature (3160°C), low thermal coefficient of expansion, extraordinary hardness, excellent wear and abrasion resistance properties [10-11]. A decrease in the reinforcement particle size from the micrometric scale to the nanometric scale results in a superior increase in the mechanical strength of the composite, but the tendency towards particle clustering and agglomeration also increases [12-14]. It is important to note that a

International Journal of Engineering Research & Technology (IJERT)
ISSN: 2278-0181
Vol. 5 Issue 01, January-2016

homogeneous distribution of reinforcing particles is essential for achieving these improved properties [15]. Mechanical alloying (MA) is a novel technique that produces bulk ultra-fine/nanostructure materials in large quantities. Many parameters influence the milling stages, such as the BPR (ball-to-powder ratio), speed, milling atmosphere, temperature, process control agent, particle size, volume fraction and reinforcement type. MA via ball milling has successfully been employed to improve the particle distribution throughout the matrix [16-18].

Various methods have been developed for MMC manufacturing. These include powder metallurgy, stir casting and the pressure infiltration method. Amongst all of the methods, powder metallurgy (P/M) is a highly developed method for the manufacture of precision metal parts. P/M technology includes the basic steps of mixing the elemental powders, compaction and sintering or heating the shape in a controlled atmosphere furnace to metallurgically bond the particles together.

The workability of a material depends purely on the amount of ductile fracture present in the material. It is influenced not only by the material microstructure, the applied temperature and the strain rate and strain but also by the stress state in the deformation zone.

Strain hardening is a property that strengthens metal through plastic deformation. This strengthening occurs because of dislocation movement and dislocation generation within the crystal structure of the material.

The cold workability and the strain hardening behaviour of aluminium, copper and iron composites, namely, Al-Al_2O_3 [19, 20], Al-Fe [21- 23], Cu-SiC [24], Fe-TiC [25], Fe-C-Mn [26] Fe-Mo [27], Al-Glass [28], Al-SiC [29] and Al-Glass-Si [30] composites, during cold upsetting under uniaxial, plane and triaxial conditions have been elaborately analysed and discussed in previous works by Narayanasamy et al. The same author also analysed the workability of Fe [31] and Fe-TiC [32] under hot upsetting. Their results have shown that the workability behaviour of metals/alloys/composites of P/M components depends on the relative density, the aspect ratio, the preform geometry, the particle size, the particle reinforcement percentage for the composites, the die geometry, the lubricants and the compacting load. The cold workability and the strain hardening behaviour of a trimodal AA 6061-10% TiO_2 nanocomposite [3] and the effects of the strengthening mechanisms on cold workability and the instantaneous strain hardening behaviour of a AA 6061-TiO_2 bimodal composite prepared by MA have been analysed in previous works by Sivasankaran et al. [3, 33]. However, the effect of TiC nanolevel reinforcement addition on AA 6061 alloy by mechanical alloying, the addition of CG matrix phase on AA 6061-TiC nanocomposite and its deformation ability were not carried out so far.

The present work aims primarily to study and investigate the morphological evaluations of trimodal AA 6061–TiCnanocomposites using optical microscopy (OM) and the effects of CG content in AA 6061–TiCnanocomposite structures on cold workability and strain hardening behaviour at room temperature.

II. MATERIALS AND METHODS

1. Powder preparation

A nanocrystalline powder of AA 6061–2wt.% TiC was produced by 30 h of MA. The matrix of the AA 6061 powder was prepared from pure elemental powders including aluminium, silicon, magnesium, iron, copper, zinc, chromium, titanium and manganese corresponding to standard Al 6061 alloy via MA. As-received pure aluminium powder with an average particle size of 7-15 µm ± 10 µm was used as the major matrix material, and the remaining alloying elements had an average particle size of less than 45 µm ± 10 µm. All of the powders were supplied by Alfa Aesar, USA. The chemical composition of the pure elemental powder required to prepare the Al 6061 alloy is 99.68Al-0.68Si-0.7Fe-0.275Cu-0.15Mn-1.0Mg-0.195Cr-0.25Zn-0.15Ti (wt.%). Titanium carbide (TiC, anatase form with octahedral structure, purity 99 %, average particle size of 75 nm ± 15 nm and 4.93 g/cc density) particles were used as a reinforcement to make composite powders. These were supplied by Sigma Aldrich, China. The MA was performed using a planetary ball mill in toluene (to avoid excessive cold welding of the powder particles) at 280 rpm with a ball-to-powder ratio of 10:1 (hardened stainless steel media) milled for up to 30 h to ensure that the process had reached a steady state. As a result, a nanocrystalline powder with an approximate 67 nm ± 8 nm crystallite size embedded with TiC nanoparticles (75 nm ± 15 nm) was obtained. In our previous work [34], details about the synthesis and the characterisation of the produced nanocomposite were investigated. To obtain the trimodal nanocomposite powders, 0, 5, 10, 15, 20, and 25 wt.% samples of the CG elemental related to AA 6061 matrix (20 µm ± 10 µm) were mechanically blended with the AA 6061-2 wt.% TiC nanocomposite powder (matrix crystallite size of 67 nm ± 8 nm) in the same ball planetary mill at 280 rpm for 2 h.

2. Compaction and sintering

Before compaction, the trimodal nanocomposite powders were dried in a N_2 atmosphere at 343 K and then consolidated using a double end die compaction technique at 500 MPa. The sampleswere30 mm in diameter, and an aspect ratio of 0.375 was obtained. The compacted green samples were degassed and then sintered at 873 K for 6 h in a N_2 atmosphere to avoid oxidation.

3. Morphological characterisation

The microstructures of the as-sintered composites were examined using an optical microscope (OM). Phase identification of the trimodal composites was performed using X-ray diffraction (XRD) with Cu-Kα radiation (1.5406 Å) in a D/Max Ultima III; XRD machine (Rigaku Corporation, Japan) operating at 30 mA and 40 KV and with a scanning range of 20°-80° in steps of 0.02.

4. Cold upsetting

The initial diameter (D_o), the initial height (h_o) and the corresponding relative density (ρ_o) of the sintered preform were measured and recorded. Each sintered preform was subjected to incremental compressive loads of 0.02 tons.

International Journal of Engineering Research & Technology (IJERT)
ISSN: 2278-0181
Vol. 5 Issue 01, January-2016

The upsetting was performed between two flat, mirror-finished open dies on a 200-ton-capacity compression testing machine. The deformation was performed until the appearance of the first visible crack was noticed on the free surface. After each interval of loading, dimensional changes in the specimen such as height after deformation (h_f), top contact diameter (D_{TC}), bottom contact diameter (D_{BC}), bulged diameter (D_B) and preform density (ρ_o) were measured and recorded. At least five readings were obtained, and the average was used for the investigation. Using the Archimedes principle, the density of the upset performs was also determined after every loading interval.

III. THEROTICAL INVESTIGATION

The workability study of the AA 6061-2 wt.% TiC nanocomposite reinforced with 0, 5, 10, 15, 20 and 25 wt.% CG Al 6061 matrix particulate trimodal nanocomposite preforms under a uniaxial stress state condition is derived using the contact and bulged diameter values of the deforming preforms during cold uniaxial upsetting. Various parameters such as the true axial strain (ε_z), the true hoop strain (ε_θ) and the true radial strain (ε_r); stresses including the true axial (σ_z), true hoop (σ_θ), true radial (σ_r), true mean or hydrostatic (σ_m) and true effective (σ_{eff}) stresses; and the stress formability index (β_σ) under a uniaxial stress state condition have been derived and discussed. The formability stress index (β_σ) parameter is useful for determining the workability of a given porous material, as described by Abdel-Rahman and El-Sheikh [35] and Narayanasamy et al. [25].

1. Stresses and strains

The uniaxial stress state condition is exhibited during upsetting under ideal conditions. Only a single stress, the axial stress (σ_z), is considered. The other stresses are considered to be zero. This pertains to the ideal stress state condition of uniaxial compression, which never prevails during the actual upsetting operation. It has been established that during the deformation of sintered P/M preforms under frictional constraints, the average density is enhanced. The presence of the friction enhances the densification, whereas the height reduction at fracture immediately decreases. The cold workability parameters under tri-axial stress state condition of powder metallurgy composite preforms, namely, the true axial stress (σ_z), the true axial strain (ε_z), the hoop strain (ε_θ), Poisson's ratio (α), relative density (R) and axial stress (σ_z), the true hoop stress (σ_θ), true hydrostatic stress (σ_m), true effective stress (σ_{eff}), the formability stress index(β_σ) *and* true effective strain (ε_{eff}) are elaborately explained from our previous works [19-32, 36] , Doraivelu et al. [37] and Vujovic et al.[38].

2. Change in dislocation densities and cold work percentage

The change in dislocation densities can be measured as [3]:

$$\frac{D_{deformed} \sim D_{undeformed}}{D_{undeformed}} = \frac{3}{2} b^2 \left(\rho_{deformed} \sim \rho_{undeformed} \right)$$

where $D_{deformed}$ & $D_{undeformed}$ are the density of composite of before and after deformation in kg/m^3 as measured by the Archimedes principle, b is the Burgers vector in m (2.86 nm for Al), and $\rho_{deformed}$ and $\rho_{undeformed}$ are the dislocation densities before and after deformation, in m^{-2}.

The percentage of cold workability (*% CW*) under an incremental load could be calculated as:

$$\%CW = \frac{100(A \sim A_0)}{A_0}$$

where A_0 and A are the initial and final cross sectional areas of the specimen. Fig. 2 shows the flow chart for determining the workability parameter and the instantaneous strain hardening index value under triaxial stress state conditions.

3. Instantaneous strain hardening behaviour

The strain hardening index value (n_i) was determined by employing the conventional Ludwik equation for the consecutive compressive loads specified as 1, 2, 3, …, (i - 1), where i is given by the following expression [20]:

$$\sigma_{eff} = K \ \varepsilon_{eff}^{n}$$

where σ_{eff} is the true effective stress, K is the strength coefficient and ε_{eff} is the true effective strain. From the above equation (17), the strain hardening index value (n_i) was derived [20]:

$$n_i = \frac{\ln\left(\frac{(\sigma_{eff})_i}{(\sigma_{eff})_{i-1}} \right)}{\ln\left(\frac{(\varepsilon_{eff})_i}{(\varepsilon_{eff})_{i-1}} \right)}$$

The strain hardening behaviour of the developed composites was studied in terms of strain hardening index (n_i), which can be determined.

IV. RESULTS AND DISCUSSION

1. Microstructure of trimodal AA 6061-TiC nanocomposite

The main objective of the microstructure evaluation is to investigate the distributions of ceramic nanoparticles (TiC) and CG phase in ultra-fine grain (UFG) Al 6061 matrix with the help of OM, backscattered scanning electron images (BSEI) and HRTEM techniques. The sintered samples were polished using emery sheets and a grinding machine using diamond paste with a size of 1 micron. After being polished, the samples were chemically etched using Keller's reagent (90 ml of distilled water + 5 ml of nitric acid + 3 ml of hydrochloric acid + 2 ml of hydrofluoric acid). Fig. 2(a)-(f) shows the optical micrograph of the trimodal nanocomposite after etching. The grey region represents UFG AA 6061 matrix reinforced with TiC nanoparticles, and the bright region represents the CG AA

International Journal of Engineering Research & Technology (IJERT)
ISSN: 2278-0181
Vol. 5 Issue 01, January-2016

6061 matrix. Fig. 2(b)-(f) clearly show the uniform distributions of the 5, 10, 20 and 25 wt.% CG matrices in the UFG matrix. It can be observed that as the percentage of CG matrix particles increased, the size of the CG domain also increased. Usually, when the trimodal material is deformed, the dislocations move a significant distance without any CG grain boundary interruption. Hence, increasing the sizes of the CG domain will impart more ductility to the material than would the corresponding UFG or NC material.

It was observed from Fig. 2(a)–(c) that the size of the CG matrix did not increase with an increase in the 10 wt.% CG phase. These results revealed that there was non-agglomeration and non-coalescence of the individual CG phases. Moreover, the average CG matrix phase size began increasing when the CG phase increased beyond 10 wt. % (Fig. 2(d)-(f)). Fig. 2(f) clearly shows a large CG phase size that resulted from the coalescence of individual CG matrix particles.

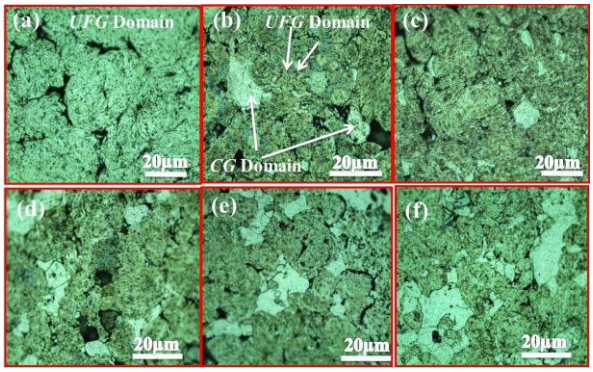

Fig. 2 Optical microstructures of as-sintered trimodal AA 6061-2 wt.% TiC nanocomposites containing x wt. % CG matrix: (a) x= 0%; (b) x= 5%; (c) x=10%; (d) x=15%; (e) x=20%; (f) x=25%.

The XRD patterns of AA 6061-TiC-x wt.% CG (x = 0, 5, 10, 15, 20 & 25 wt.%) trimodal nanocomposites are shown in Fig. 3(a). The XRD results revealed an increase in the intensity of the Al matrix peaks as the wt. % of the CG content increased. An increase in intensity and a slight decrease in peak width were observed to be more for the 25 wt.% CG nanocomposite than for the 0 wt.% CG nanocomposite (Fig. 3(b)). These results indicated that there was less distortion in the matrix structure. This was expected to improve the ductility of the nanocrystallite matrix. Similar results were obtained by the previous study [3].

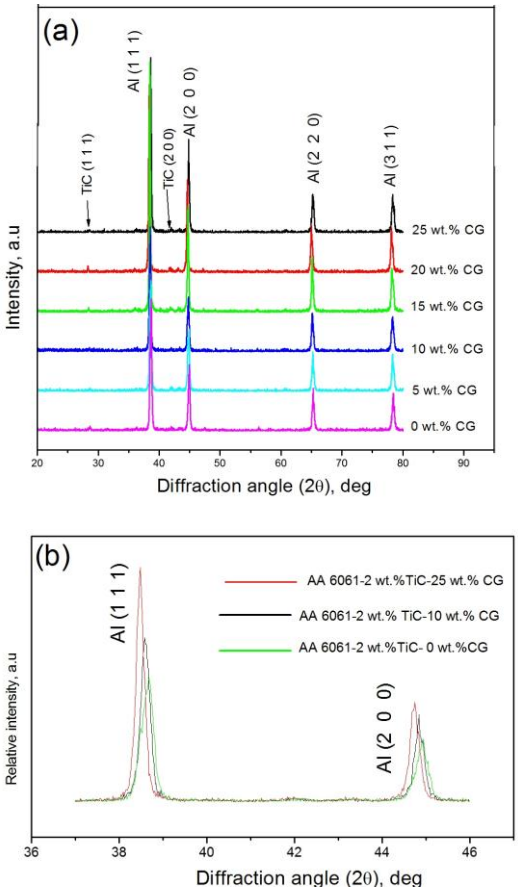

Fig. 3 XRD patterns of: (a) AA 6061- 2 wt. % TiC-x wt. % CG trimodal nanocomposite powders (x=0, 5, 10, 15, 20 and 25 wt.%); (b) The inset shows the shift in the Bragg angle.

2. Workability behaviour of stresses on trimodal nanocomposite perform

Fig. 4(a)–(c) has been plotted between various triaxial stresses, namely, the true axial stress (σ_z), the true mean or hydrostatic stress (σ_m) and the true effective stress (σ_{eff}) with the true effective strain (ε_{eff}) for trimodal composites containing various CG weight percentages at room temperature. As shown in Fig. 4(a), it was observed that there was a poor strain hardening region with a true effective strain of approximately 3.9% that exhibited the highest axial stress of 180 MPa. This was because the dispersoid of TiC nanoparticles and the UFG matrix interface de-cohesion might have a detrimental effect. However, as the CG matrix percentage increased from 5 to 10, the maximum axial stress began to increase, and the 10 wt.% CG matrix exhibited a maximum axial stress of 260 MPa and 6.5% compressive ductility. As the percentage of the CG matrix in the UFG matrix increased, the CG phase attempted to accommodate the dislocation mobility. In addition, the CG phase arrested the crack propagation that occurred in the NC or UFG material. The maximum axial stress of the 10 wt.% CG matrix preform exhibited 44% more value than did the 0 wt.% CG or UFG composites. This is attributed to the improved densification of the composite as the soft phases in the structure increased. It was further expected that an effective load transfer would occur in the multi-scale microstructure (i.e., load transfer from the CG phase to the UFG phase) and the non-

International Journal of Engineering Research & Technology (IJERT)
ISSN: 2278-0181
Vol. 5 Issue 01, January-2016

coalescence of individual CG matrix particles (Fig. 2(c)). However, as the CG matrix phase increased in the UFG matrix beyond 10 wt.%, the axial stress decreased. This was attributed to the domination of the CG phase softness because of coalescence that resulted in a decrease in the load transfer rate. The 25 wt.% CG composites exhibited a considerable compressive ductility of approximately 11%, which was 2.82 times higher than the 0 wt.% CG composites. The improvement in compressive ductility for the 25 wt.% CG composites was attributed to the high proportion of the CG phase in the nanocomposites, which may effectively delay crack initiation from the UFG matrix during deformation. In other words, as the soft CG matrix in the UFG composite was plastically deformed, the dislocation density increased within the CG phase. The barrier-like grain boundary arrested these dislocation movements. Therefore, more work, or strain hardening, occurred. This deformation would be useful for closing the pores to some extent, which can enhance the densification of UFG composites. Therefore, a 25 wt.% CG composite exhibited considerable compressive ductility while maintaining reasonable strength and toughness. Fig. 4(b) shows the variation of the true hydrostatic stress with true effective strain in the 0, 5, 10, 15, 20 and 25 wt.% CG matrices. It is well known that the specific surface area of the material increases as the grain sizes are reduced from the micron level to an ultra-fine level or nano level. As a result, a large number of grain boundaries are formed [39]. In other words, the particle mass-to-surface area ratio decreased during grain refinement, which promoted inter-particle friction effects. This inter-particle friction effect decreased the composite density during cold uniaxial compaction [3]. The porosity level of the 0 wt.% CG composite was high, the true hydrostatic stress increased steeply with far less deformation when compared with the 25 wt.% CG shown in Fig. 4(b). It was also observed that as the percentage of CG increased from 0 wt.% to 15 wt.%, the true hydrostatic stress increased gradually, with small changes in the true effective strain. After 15 wt.% CG, the true hydrostatic stress increased slightly as the true effective strain increased. Additionally, the CG phase produced lateral flow as the CG phase increased. It finally fractured with a high true effective strain for 25 wt.% CG composite. Therefore, good formability was obtained for the 25 wt.% CG composite while maintaining considerable strength.

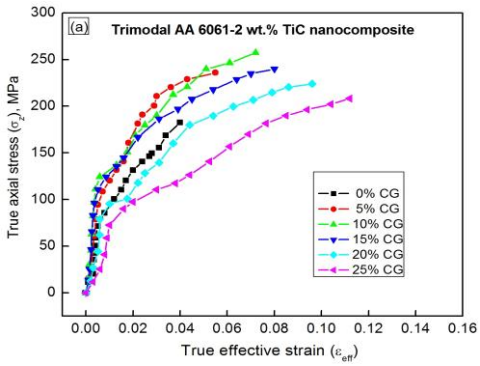

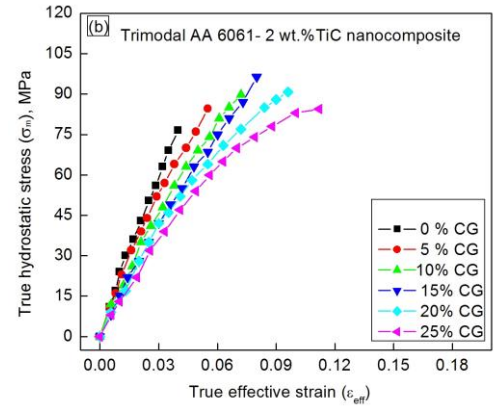

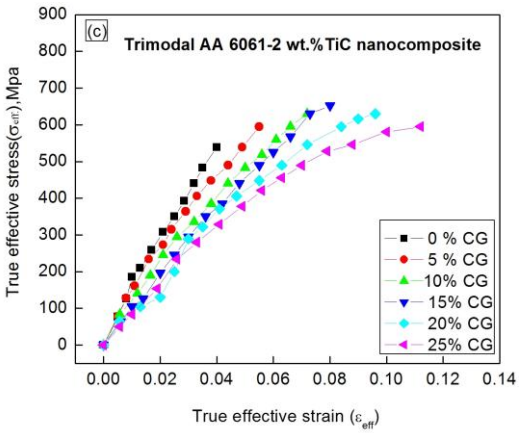

Fig. 4 (a) Variation in true axial stress; (b) Variation in true hydrostatic stress; (d) Variation in true effective stress with true effective strain.

Fig. 4(c) shows the variation in the true effective stress with the true effective strain. After cold upsetting, the true effective stress was calculated and it was found that the true effective stress increased gradually with true effective strain from 0 wt.% to 15 wt.% CG. For 15 wt.% CG, an ultimate compressive strength of 670 MPa was determined, which was 2.5 times higher than that of the conventional coarse grain [29]. It is also only 30% and 50% less than that of the mechanical alloys [3] (MA 30% CG AA 6061-10 wt.% TiO_2, 935 MPa) and cryo-milled materials [5] (CM of 50% CG AA 5083-B_4C composite 1070 MPa). It was previously determined that these nanocomposites exhibited high strength but poor workability and compressive ductility [3]. The ultimate compressive strengths for 0, 5, 10, 15, 20 and 25 wt.% CG are 539, 595, 630, 670, 630 and 595 MPa, respectively. This investigation showed that the compressive strength increased up to 15 wt.% CG because of the non-coalescence of individual CG matrix particles and because of the almost uniform distribution of the CG phase in the UFG matrix before decreasing to 25 wt.% CG, which was because of the coalescence of individual CG matrix particles. The same phenomenon was observed in an earlier study [3].

3. Workability behaviour of the formability stress index (β) on trimodal nanocomposites

Fig. 5 shows the plot between the formability stress index and the true effective stress. It was observed that the formability stress index increased steadily with the CG

International Journal of Engineering Research & Technology (IJERT)
ISSN: 2278-0181
Vol. 5 Issue 01, January-2016

content in the NC or the UFG matrix because of the introduction of a soft CG parent phase in the UFG matrix. The CG band developed a lateral flow as the CG content increased. The maximum formability stress index for 25 wt.% CG is 0.497, which was 55% higher than that of 0 wt.% CG (0.32). This was because of the plastic deformation in the CG matrix particles.

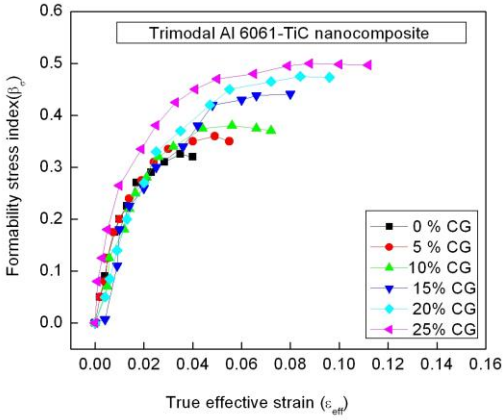

Fig. 5 Variation in the formability stress index with true effective strain for various CG contents.

4. Change in dislocation density, fracture limit strain and the percentage of cold workability

Fig. 6(a) shows the variation in the change in dislocation density and fracture limit strain with different wt.% of CG contents. The changes in dislocation density increased gradually from 0 wt.% CG to 25 wt.% CG, and the maximum plastic deformation occurred in the trimodal nanocomposite for the case of 25 wt.% CG compared with the 0 wt% CG case. A previous work by Sivasankaran et al. explains the reason behind the increase in plastic deformation. Additionally, the fracture limit strain value increased as the % of CG content increased in the trimodal nanocomposite because the plastic deformation region increased. Fig. 6(b) shows the variation of percentage cold workability with various CG contents. The maximum percentage of cold workability was found in the case of 25 wt.% CG, where it was approximately 450% greater than that of the 0 wt.% CG nanocomposite. After investigation, the 25 wt.% CG nanocomposite showed a maximum workability and strain hardening value when compared with others without sacrificing strength.

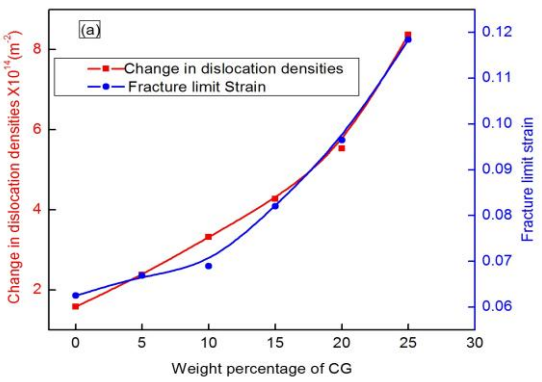

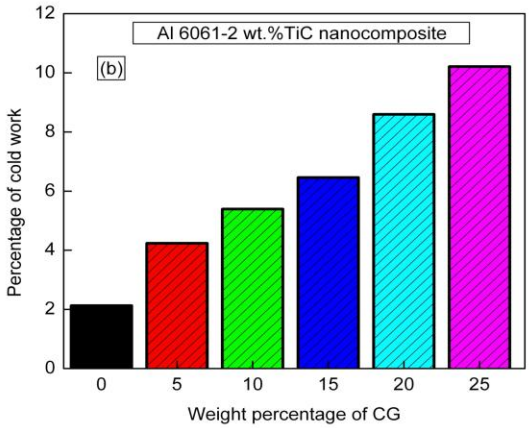

Fig. 6 (a) Variation in the change in dislocation densities and fracture limit strain with different CG contents (b) Variation in percentage of cold work with different CG contents.

5. Strain hardening behaviour of trimodal nanocomposites

Fig. 7 shows the plot between instantaneous strain hardening and true effective strain with different wt.% of the CG matrix. From this plot, it can be observed that the instantaneous strain hardening value increases steeply with lower or negligible deformation while increasing to a maximum value at 0.012 (true effective strain). The index value also increased as the CG wt.% increased, and a maximum value of 0.652 was achieved at 15 wt.% CG. However, beyond 15 wt.% CG, the index value decreased slightly because of increasing softness and because of the reduction in hard ceramic particles in the trimodal nanocomposite. For the 0 wt.% CG matrix, poor compressive ductility and toughness (area under the curve) can be clearly observed. This was a result of the higher segregation of minor solute atoms to the Al UFG during sintering and because of the high amount of stored energy in the Al matrix. The case with 25 wt.% CG resulted in the maximum compressive ductility and toughness compared with the others. It was also found that a delay occurred in the plastic instability as the wt.% of CG content increased in the trimodal nanocomposite. A desirable instantaneous strain hardening behaviour was observed in the 25 wt.% CG composite because of the lower solute content or because of the interstitial elements in UFG matrix after sintering. From Fig. 7, it was concluded that the 25 wt.% CG composite resulted in considerable matrix work hardening (i.e., work hardening of the Al matrix) and geometry work hardening (i.e., improved density because of the soft CG phase). As a result, this composite had excellent formability.

International Journal of Engineering Research & Technology (IJERT)
ISSN: 2278-0181
Vol. 5 Issue 01, January-2016

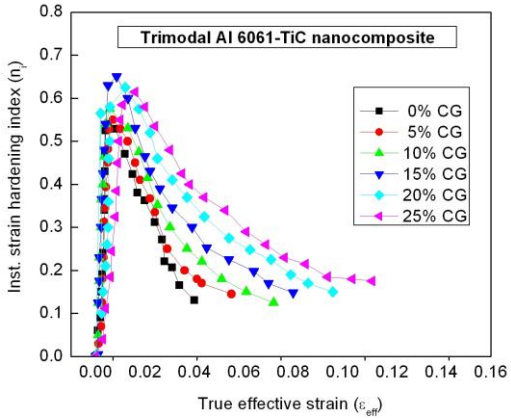

Fig. 7 Variation in the instantaneous strain hardening index with the true effective strain.

V. CONCLUSIONS

A trimodal nanocomposite can be successfully fabricated using MA. The homogeneous distribution of a hard ceramic phase and a CG phase was confirmed using different morphological evaluation methods. The cold upsetting test was conducted at room temperature, and different parameters that showed the performance of trimodal nanocomposites were investigated.

- The addition of CG content retards micro crack nucleation during deformation and also improves the compressive ductility and delays the plastic instability.
- The strain hardening index value (n_i) increases as the CG content increases from 0 wt.% to 15 wt.% because of decreasing pore sizes. Furthermore, the increase of the CG content to 25 wt.% resulted in a slight decrease of the strain hardening index value. This decreased the geometric work hardening and increased the matrix work hardening.
- Addition of 15 wt.% CG to Al 6061-2 wt.% TiC resulted in a higher strain hardening index (n_i) and a higher strength coefficient (K) values because of the resulting better load transfer rates.
- The formability stress index ($\beta\sigma$) increases as the CG wt.% increases because of better densification and decreased pore size. The 25 wt.% CG composite also showed a higher percentage of cold workability and therefore possessed a high formability stress index value when compared with the other composites.
- A high compressive ductility was obtained for the case of 25 wt.% CG as compared with the 0 wt.% CG case. The ultimate compressive strength for the 25 wt.% CG nanocomposite was 595 MPa, which was only 12% lower than that of the 15 wt.% CG (670 MPa). The formability stress index value was 0.32 for 0 wt.% CG material and 0.497 for 25 wt.% CG material. The value for the 25 wt.% CG material was 55% higher than that of the 0 wt.% CG material. This shows that a high % of cold workability was obtained for the 25 wt.% CG material compared with the other nanocomposite.

ACKNOWLEDGEMENTS

The authors wish to express their gratitude to the General Manager and the Joint General Managers, Heavy Alloy Penetrator Project (HAPP), Tiruchirappalli, Tamilnadu, India, for permitting them to utilise the powder metallurgy shop facilities for the present work.

REFERENCES

[1] Sivasankaran S, Sivaprasad K, Narayanasamy R, Vijay Kumar Iyer. Synthesis, structure and sinterability of 6061 AA100−x–xwt.% TiO_2 composites prepared by high-energy ball milling. J Alloys Compd 2010; 491:712-21

[2] Miracle DB. Metal matrix composites-From science to technological significance. Compos Sci Technol 2005; 65 (15–16): 2526–40.

[3] Sivasankaran S, Sivaprasad K, Narayanasamy R. Microstructure, cold workability and strain hardening behavior of trimodaled AA 6061–TiO_2nanocomposite prepared by mechanical alloying. Mater Sci and Eng A 2011; 528:6776-87.

[4] Lee Z, Witkin DB, Radmilovic V, Lavernia EJ, Nutt SR. Bimodal microstructure and deformation of cryomilled bulk nanocrystalline Al-7.5 Mg alloy. Mater Sci Eng A 2005; 410–411: 462–67.

[5] Ye J, Han BQ, Lee Z, Ahn B, Nutt SR, Schoenung JM. A tri-modal aluminum based composite with super-high strength. Scr Mater 2005; 53: 481–86.

[6] Yao B, Hofmeister C, Patterson T, Sohn Y, Bergh MVD, Delahanty T et.al. Microstructural features influencing the strength of Trimodal Aluminum Metal-Matrix-Composites. Compos A 2010; 41:933–41.

[7] Linli Zhu, Jian Lu. Modelling the plastic deformation of nanostructured metals with bimodal grain size distribution. Int J Plasticity 2012; 30-31:166-184

[8] Witkin D, Lee Z, Rodriguez R, Nutt S, Lavernia E. Al-Mg alloy engineered with bimodal grain size for high strength and increased ductility. Scr Mater 2003; 49:297–302.

[9] Wang Y, Chen M, Zhou F, Ma E. High tensile ductility in a nanostructured metal. Nature 2002; 419: 912–15.

[10] Wang Y, Rainforth WM, Jones H, Lieblich M. Dry wear behaviour and its relation to microstructure of novel 6092 aluminium alloy–Ni3Al powder metallurgy composite. Wear 2001; 251:1421–32.

[11] Salem H, El-Eskandarany SH, Kandil A, Abdul Fattah H. Bulk behavior of ball milled AA2124 nanostructured powders reinforced with TiC. J Nanomater. Hindawi Publishing Corporation; 2009. 12 p. [Article ID 479185].

[12] Khor KA, Cao Y, Boey FYC, Hanada K, Murakoshi Y, Sudarshan TS et.al. Processing and response of aluminum-lithium alloy composites reinforced with copper-coated silicon carbide particulates. J Mater Eng Perform 1997; 7:66-70.

[13] Tan MJ, Zhang X. Powder metal matrix composites: selection and processing. Mater Sci Eng A 1998; 244:80–85.

[14] Fogagnolo JB, Robert MH, Torralba JM. Mechanically alloyed AlN particle reinforced Al-6061 matrix composites, powder processing, consolidation and mechanical strength and hardness of the as-extruded materials. Mater Sci Eng A 2006; 426:85–94.

[15] Khakbiz M, Akhlaghi F. Synthesis and structural characterization of Al–B_4C nano-composite powders by mechanical alloying. J Alloy Compd 2009; 479:334–41.

[16] Mohammad Sharifi E, Karimzadeh F, Enayati MH. Mechanochemically synthesized Al_2O_3-TiC nanocomposite. J Alloy Compd 2010; 491:411-15.

[17] Zakeri M, Yazdani-Rad R, Enayati MH, Rahimipoor MR. Synthesis of $MoSi_2$–Al_2O_3nanocomposite by mechanical alloying. Mater Sci Eng A 2006; 430:1-2:185–88.

[18] Razavi Hesabi Z, Hafizpour HR, Simchi A. An investigation on the compressibility of aluminum/nano-alumina composite powder prepared by blending and mechanical milling. Mater Sci Eng A 2007; 454–455:89–98.

[19] Narayanasamy R, Ramesh T, Pandey KS. Workability studies on cold upsetting of Al-Al_2O_3 composite Material. Mater Des 2006; 27:566–75.

[20] Narayanasamy R, Anandakrishnan V, Pandey KS. Effect of geometric work-hardening and matrix work-hardening on workability and densification of aluminium-3.5% alumina composite during cold upsetting. Mater Des 2008; 29 (8):1582–99.

International Journal of Engineering Research & Technology (IJERT)
ISSN: 2278-0181
Vol. 5 Issue 01, January-2016

[21] Narayanasamy R, Ramesh T, Pandey KS. Some aspects on cold forging of aluminium-iron powder metallurgy composite under triaxial stress state condition. Mater Des 2008; 29(4):891–903.
[22] Narayanasamy R, Selvakumar N, Pandey KS. Phenomenon of instantaneous strain hardening behavior of sintered Al-Fe composite performs during cold axial forming. Mater Des 2007; 28 (4):1358-1363.
[23] Narayanasamy R, Ramesh T, Pandey KS, Pandey SK. Effect of particle size on new constitutive relationship of aluminum-iron powder metallurgy composite during cold upsetting. Mater Des 2008; 29 (5):1011–26.
[24] Sumathi M, Selvakumar N, Narayanasamy R. Workability studies on sintered Cu-10 SiC performs during cold axial upsetting. Mater Des 2012; 39:1-8
[25] Narayanasamy R, Senthilkumar V, Pandey KS. Some aspects of workability studies on P/M sintered high strength 4% titanium carbide composite steel performs during cold upsetting. Mater Des 2006; 3: 39-57.
[26] Mohan Raj AP, Selvakumar N, Narayanasamy R, Kailasanathan C. Experimental investigation on workability and strain hardening behaviour of Fe-C-Mn sintered composites with different percentage of carbon and manganese content. Mater Des 2013; 49:791-801.
[27] Narayanasamy R, Anandakrishnan V, Pandey KS. Effect of molybdenum addition on workability of powder metallurgy steels during cold upsetting. Mater Sci Eng A 2009; 517: 30-36
[28] Kumar DR, Loganathan C, Narayanasamy R. Effect of glass in aluminum matrix on workability and strain hardening behavior of powder metallurgy composite. Mater Des 2011; 32:2413-22.
[29] Narayanasamy R, Ramesh T, Prabhakar M. Effect of particle size of SiC in aluminum matrix on workability and strain hardening behaviour of P/M composite. Mater Sci Eng A 2009; 504:13–23.
[30] Kumar DR, Narayanasamy R, Loganathan C. The Effect of Glass and SiC in Aluminum matrix on workability and strain hardening behavior of powder metallurgy hybrid composites. Mater Des 2012; 34:120-36.
[31] Narayanasamy R, Senthilkumar V, Pandey KS. Some aspects on hot forging features of P/M sintered iron performs under various stress state condition. Mech Mater 2006; 38: 367-86.
[32] Narayanasamy R, Senthilkumar V, Pandey KS. Some aspects of workability studies on hot forging of sintered high strength 4% titanium carbide composite steel performs Mater Sci Eng A 2006; 425: 121-30.
[33] Sivasankaran S, Sivaprasad K, Narayanasamy R, Vijay Kumar Iyer. Effect of strengthening mechanisms on cold workability and instantaneous strain hardening behavior during grain refinement of AA 6061-10 wt.% TiO_2 composite prepared by mechanical alloying. J Alloys and Compd 2010; 507:236-44.
[34] Jeyasimman D, Sivasankaran S, Sivaprasad K, Narayanasamy R, Kambali RS. An investigation of synthesis, consolidation and mechanical behaviour of Al 6061 nanocomposites reinforced by TiC via mechanical alloying. Mater Des 2014; 57: 394-404.
[35] Abdel-Rahman M, El-Sheikh MN. Workability in forging of powder metallurgy compacts. J Mater Process Technol 1995; 54:97-102.
[36] Narayanasamy R, Ramesh T, Pandey KS. Some aspects on workability of alminium-iron powder metallurgy composite during cold upsetting. Mater Sci Eng A 2005; 391 (1-2):418-26.
[37] Doraivelu SM, Gegel HL, Gunasekara JS, Malas JC, Morgan JT, Thomas Jr. JF. A new yield functions for compressible PM materials. Int J Mech Sci 1984; 26;527-35.
[38] Vujovic V, Shabaik AH. New workability criteria for ductile metals. J Eng Mater Technol Trans ASME 1986; 108(3):245–49.
[39] C.Suryanarayana, Mechanical alloying, Powder Metal Technologies and Applications, Vol 7, ASM International, 1998; 7:80-90.